Chemical bonding in $V(TCNE)_x$ ($x \sim 2$) thin-film magnets grown *in situ*

M. P. de Jong,[1] C. Tengstedt,[2] A. Kanciurzewska,[2] E. Carlegrim,[2] W. R. Salaneck,[1] and M. Fahlman[2]
[1]*Department of Physics (IFM), Linköping University, S-581 83 Linköping, Sweden*
[2]*Department of Science and Technology (ITN), Linköping University, S-601 74 Norrköping, Sweden*
(Received 8 September 2006; revised manuscript received 14 December 2006; published 6 February 2007)

The molecule-based magnet $V(TCNE)_x$, with TCNE=tetracyanoethylene, $x \approx 2$, shows an exceptionally high magnetic ordering temperature of about 400 K. With the aim to shed light on the origins of the robust magnetic ordering interactions, we have characterized the chemical bonding in $V(TCNE)_x$ thin films, prepared by an *in situ* chemical vapor deposition method, using photoelectron spectroscopy, x-ray absorption spectroscopy (XAS), and x-ray magnetic circular dichroism (XMCD). The XAS and XMCD results were interpreted by ligand field multiplet and charge transfer multiplet calculations, which show that the V-NC bonds are characterized by a large crystal field parameter $10Dq=2.3$ eV and strong ligand to metal charge transfer effects, resulting in a hybrid V($3d$)-CN ground state given by 60% $3d^3$ and 40% $3d^4L$, where L is a hole on the cyano ligands.

DOI: 10.1103/PhysRevB.75.064407 PACS number(s): 75.25.+z, 73.61.Ph, 79.60.Fr

I. INTRODUCTION

Within the extensive scope of magnetic materials available at present, magnets based on organic molecules form a unique class.[1–3] In metalo-organic molecule-based magnetic complexes, the organic building block plays a key role, which can either be passive by mediating the magnetic interaction, or active, in case the organic part carries a net spin. In the latter case, a significant fraction of the ordered spins resides in $p(\pi)$ orbitals, in contrast to the d and f spins found in conventional, inorganic magnets.

From a technological point of view, molecule-based magnets offer many potential advantages over conventional metal and ceramic magnets.[4] Their properties can be modulated via chemical routes, and they are lighter, more flexible, and much less energy intensive to produce. Moreover, insulating and semiconducting behavior can readily be obtained. These and other attributes make these systems attractive for, e.g., spin electronics, or spintronics (see Ref. 5).

As prototypical magnets, transition metal-tetracyanoethylene (M-TCNE) complexes,[6] containing, e.g., V, Mn, Fe, Ni or a mixture of such metals, are particularly interesting since they span a large range of relatively high magnetic ordering temperatures and show various kinds of complex magnetic behavior. For example, for $M(TCNE)_x \cdot y(CH_2Cl_2)$ ($x \sim 2$, $y \sim 1/2$) compounds with M =Mn,[7] Fe,[8] or V,[9] the critical temperatures are T_C=75 K, 97 K, and ~400 K, respectively. It should be noted that the latter value was obtained by a debatable extrapolation above the decomposition temperature of the compound at ~350 K (see, e.g., Ref. 10 and references therein), at a later stage the high T_C values were confirmed for solvent free $V(TCNE)_x$.[11] While $Mn(TCNE)_x \cdot y(CH_2Cl_2)$ shows random exchange and reentrant spin glass behavior, evidenced by a transition from a ferrimagnetic state to a spin glass near 10 K,[7] $Fe(TCNE)_x \cdot y(CH_2Cl_2)$ features a mixture of ferrimagnetic and random anisotropy characteristics. For $V(TCNE)_x \cdot y(CH_3CN)$ with $x \sim 1.5$, $y \sim 2$ the magnetic behavior is mainly governed by random anisotropy as well.[12] So far, the physical origin of the exceptionally high T_C of the V-based materials as compared to other M-TCNE compounds is not well understood. This is largely due to the extreme air sensitivity and amorphousness of V-TCNE compounds, which has made experimental analysis (of, e.g., the electronic structure) cumbersome.

Thin films of $V(TCNE)_x$ prepared by solvent-free chemical vapor deposition (CVD) of TCNE and $V(CO)_6$ show increased structural order[11] and improved air stability,[13] although surface oxidation still occurs.[13] We have recently developed a method based on CVD in ultrahigh vacuum (UHV) to deposited contamination-free thin films of $V(TCNE)_x$, which enabled studies of the (valence) electronic structure.[14] These films were magnetically ordered at room temperature, as was verified by the observation of a large x-ray magnetic circular dichroism (XMCD) signal at the V $L_{2,3}$ edge. By means of resonant photoemission (RPE) spectra recorded at the C, N, and V x-ray absorption edges, the V($3d$) contribution to the frontier valence electronic levels could be clearly distinguished. In contrast with a previously proposed model,[15,16] describing $V(TCNE)_x$ as a completely spin polarized, half semiconducting solid in which the energy gap lies between two $TCNE^-$ derived π^* subbands, the V($3d$) states were found to be located *at the valence band edge*,[14] underlining the importance of the V($3d$) electrons for charge transport and magnetoresistance.

In the present paper, we present a detailed analysis of the chemical and electronic structure of a series of *in situ* prepared $V(TCNE)_x$ thin films, with the aim to shed light on the chemical bonding interactions in the $V(TCNE)_x$ compound. The films were studied with photoelectron spectroscopy (PES), x-ray absorption spectroscopy (XAS), and XMCD.

II. EXPERIMENT

Thin films of $V(TCNE)_x$ ($x \approx 2$, thickness 5–15 nm) were prepared by chemical vapor deposition of TCNE and $V(C_6H_6)_2$, using a custom built, UHV-compatible CVD source. The precursors were allowed to condensate and react simultaneously on sputter-cleaned gold substrates at room

temperature. No film formation was observed for deposition of the precursors alone, while co-deposition resulted in reproducible film growth of $V(TCNE)_x$. In order to study the effects of (mild) oxidation during growth, the base pressure in the deposition chamber was varied between 10^{-6} and 10^{-8} mbar.

A series of $V(TCNE)_x$ films was characterized with x-ray and ultraviolet photoelectron spectroscopy (XPS and UPS), using an UHV spectrometer of our own design (base pressure $\sim 10^{-10}$ mbar). This system is equipped with a hemispherical electron energy analyzer, a monochromatized He resonance lamp for UPS (HeI $h\nu = 21.2$ eV or HeII $h\nu = 40.8$ eV), and a nonmonochromatized Al(K_α) x-ray source for XPS ($h\nu = 1486.6$ eV). The resolution for the UPS measurements is 0.1 eV, as was determined from the Fermi-edge of an Au reference sample. The XPS resolution is 1.2 eV, obtained from the full width at half maximum of the Au($4f_{7/2}$) core-level line.

PES, XAS, and XMCD experiments were carried out on a second series of *in situ* prepared films at beamline D1011 of the MAX-II storage ring of the MAX-Laboratory for Synchrotron Radiation Research in Lund, Sweden. The end station is equipped with a Scienta SES-200 hemispherical electron energy analyzer, and a purpose built microchannel plate (MCP) detector for electron yield measurements. An incident angle $\theta = 70°$ of the photon beam relative to the sample normal was used for the XAS and XMCD measurements. For PES, the spectra were recorded with the electron emission direction along the sample normal, for which $\theta = 50°$. The angular acceptance of the spectrometer was set to about 10°, while the electron energy resolution was about 100 meV. For $h\nu < 300$ eV, the photon linewidth was kept below ~50 meV. At higher photon energies, a linewidth of ~100 meV was used to keep the photon flux sufficiently high. Calibration of the photon energies and the electron binding energies was carried out using a procedure described elsewhere.[17] The XMCD measurements were performed at room temperature with opposing directions of in-plane magnetization and with fixed helicity of the incident light. The samples were magnetized with a ~200 G magnetic field pulse, while the XAS and XMCD spectra were recorded in remanence.

III. RESULTS AND DISCUSSION

A. Core level analysis

Information about the elemental composition and chemical structure of the $V(TCNE)_x$ films is contained in the XPS core-level spectra. We will start with an analysis of the composition of the compound, followed by a discussion of the various core-level peak positions and shapes, as compared to previous studies of *ex situ* CVD-grown films,[13] and to XPS analysis of two model compounds: pure condensed TCNE, and condensed TCNE intercalated with rubidium. The latter is a well characterized ionic charge transfer complex, containing $TCNE^-$ molecules and Rb^+ counterions.[18]

Analysis of the C($1s$), N($1s$), and V($2p$) peak intensities shows that the carbon to nitrogen ratios of "oxygen free"

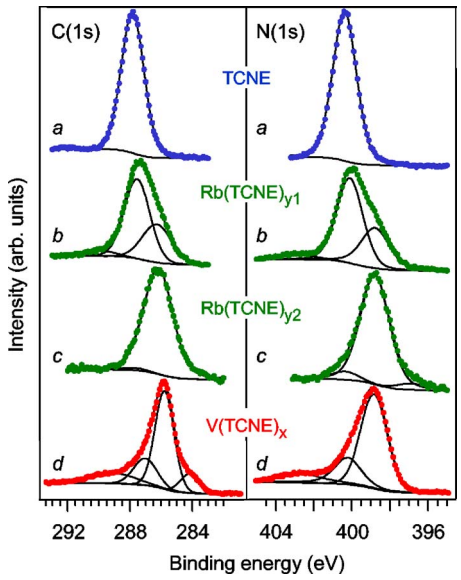

FIG. 1. (Color online) C($1s$) and N($1s$) XPS spectra of (a) TCNE, (b) Rb-intercalated TCNE with intermediate Rb concentration, denoted $Rb(TCNE)_{y1}$, (c) Rb-intercalated TCNE with high Rb concentration, denoted $Rb(TCNE)_{y2}$, (d) $V(TCNE)_x$.

$V(TCNE)_x$ films are, as expected, similar to those of pure, physisorbed TCNE films, prepared by vapor deposition on gold substrates kept at −180 °C. In the oxygen free $V(TCNE)_x$ films, prepared with a base pressure of 10^{-8} mbar in the deposition chamber, only traces of oxygen could be detected on the order of the XPS detection limit of ~0.1 at. %, while the oxygen concentration amounted to about 3 at. % when the base pressure was increased to 2×10^{-6} mbar. The nitrogen to vanadium ratio $R_{NV} = 7.5$, calculated from the N($1s$) and V($2p$) signals using standard atomic sensitivity factors,[19] suggests that two TCNE molecules share one vanadium ion. This is in excellent agreement with the composition $V^{2+}(TCNE)^-_x$ with $x = 2$, which is also fully consistent with the other experimental findings discussed below.

The N($1s$) core level spectra of $V(TCNE)_x$, TCNE and Rb-intercalated TCNE are depicted in Fig. 1 (right panel), with the corresponding curve fits (performed with XPSPEAK 4.1) using Shirley backgrounds and Voigt (nearly Gaussian) peak shapes. The features present in the Rb-intercalated TCNE films were previously assigned,[18] from high to low binding energy, to: shake up, neutral TCNE, and singly negatively charged molecules, $TCNE^-$. The weak signal at about 396.5 eV was tentatively assigned to be due to additional screening from neutral rubidium, upon island growth of excessive Rb atoms. The position of the N($1s$) peak of $V(TCNE)_x$ is identical to that of the $TCNE^-$ derived peak of Rb-intercalated TCNE, whereas the asymmetrical peak profile, accounted for by two peaks in the curve fit, could be taken as an indication for the presence of neutral TCNE. An analogous assignment was previously given by Pokhodnya *et al.*, who observed a N($1s$) peak of similar appearance and binding energy position for *ex situ* $V(TCNE)_x$ prepared by CVD growth from TCNE and $V(CO)_6$ precursors.[13] It was claimed that the high binding energy component, at about

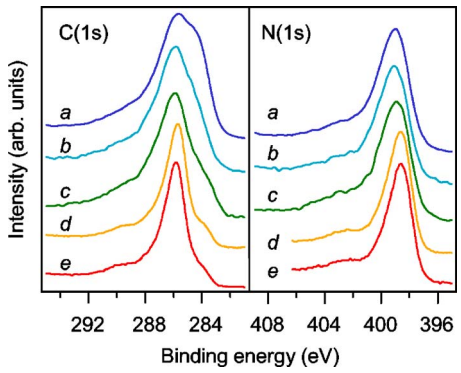

FIG. 2. (Color online) C(1s) and N(1s) XPS spectra of V(TCNE)$_x$ films deposited at base pressures varying from 10^{-6} mbar (a), 10^{-7} mbar (b), $\sim 5 \times 10^{-8}$ mbar (c) to 10^{-8} mbar (d) and (e). The inclusion of adventitious carbon at low base pressures can be observed from the growth of a low binding energy feature.

400.1 eV, strongly gained intensity upon air exposure, strengthening the assignment to neutral TCNE which is formed upon oxidation of $TCNE^-$. However, the *in situ* prepared films do not contain a significant amount of oxygen, and even for those films that were mildly oxidized during growth (containing several at. % oxygen), the N(1s) feature remained unaffected (see Fig. 2, right panel). It should be noted that the N(1s) and C(1s) spectra of Fig. 2 labeled (a), (b), and (c), were recorded in our home laboratory, while spectra (d) and (e) were measured in MAX-lab. Hence, the resolutions are different, and the peak positions differ slightly due to energy calibration errors, which leads to an artificial small peak shift between those groups of spectra. Since mild oxidation has no influence on the N(1s) spectra, we propose that the asymmetry of the N(1s) feature is not related to the presence of neutral TCNE, but is due to inequivalent bonding environments of the cyano groups. Recently, extended x-ray absorption fine structure studies have been performed by Haskel *et al.* to probe the local structure of the vanadium ion,[20] showing a coordination environment involving 6.04 ± 0.25 nitrogen atoms. For a composition of $V^{2+}(TCNE)^-_2$, some nitrogen atoms must remain uncoordinated since each TCNE molecule contains four N atoms. The presence of uncoordinated cyano groups in addition to those bonded to V^{2+} ions may very well lead to the observed chemical shifts on the order of 1 eV. Moreover, disorder in the films could lead to a variety of bonding configurations, e.g., containing both twisted and planar TCNE molecules,[10] leading to a distribution of N(1s) binding energies. Regardless of the exact origin of the peak asymmetry, it can be concluded that the majority of N-atoms carry a similar amount of charge as those in Rb-intercalated TCNE, consistent with the predominant species being $TCNE^-$ in V(TCNE)$_x$.

Figure 1 (left panel) shows the C(1s) XPS spectra of V(TCNE)$_x$ and the model compounds. The C(1s) case largely mimics what was found for N(1s), but an additional feature at low binding energy (at 284 eV) is present for V(TCNE)$_x$, which is assigned to benzene-related impurities originating from $V(C_6H_6)_2$. Upon increasing the background pressure of residual gases during deposition, a clear increase of this low binding energy feature is observed, along with the incorporation of a significant amount of adventitious carbon, see Fig. 2 (left panel). This shows that oxidation products of $V(C_6H_6)_2$ are included in the films at poor background pressures, resulting in an increase of the benzene-related signal and a higher overall carbon content. It should be pointed out that the shoulder at 284 eV is never completely suppressed, even for oxygen-free films, indicating that a small amount of benzene-derived impurities is intrinsic to the V(TCNE)$_x$ films.

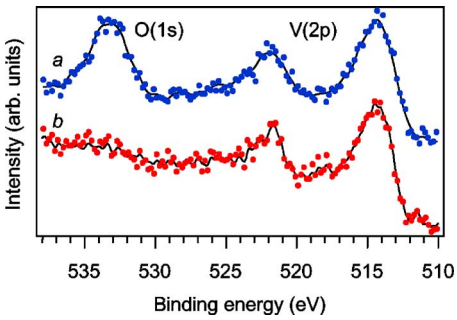

FIG. 3. (Color online) V(2p) and O(1s) XPS spectra of V(TCNE)$_x$ films deposited at 10^{-6} mbar (a) and 10^{-8} mbar (b).

Figure 3 depicts XPS spectra of the O(1s) and V(2p) features, obtained for films prepared with 10^{-8} mbar (bottom curve) and 10^{-6} mbar (top curve) base pressures in the deposition chamber. In both spectra only a single V(2p) doublet is observed, situated at 513.9 eV [V(2p)$_{3/2}$] and 521.5 eV [V(2p)$_{1/2}$], similar to the low binding energy components in the V(2p) XPS spectra obtained by Pokhodnya *et al.* that were assigned to V^{2+}.[13] Indeed, the binding energy values are in good agreement with those of V^{2+} in vanadium oxides.[21]

B. Valence electronic structure

We briefly revisit the valence band electronic structure, which we have discussed in more detail in an earlier publication within the context of PES and RPE studies.[14] Figure 4 displays valence band PES spectra, recorded at two different photon energies (21.2 eV, panel A, and 40.8 eV, panel B), of thin films of condensed TCNE, TCNE intercalated with rubidium, and V(TCNE)$_x$.

The isolated peak at 5.6 eV in the TCNE spectra is related to the highest occupied molecular orbital (HOMO). In Rb-intercalated TCNE, electron transfer from Rb atoms to the TCNE molecules gives rise to two distinct peaks in the frontier electronic structure, corresponding to the destabilized former HOMO (at 3.5 eV) and a singly occupied molecular orbital (SOMO, at 1.5 eV) formed by stabilizing the LUMO of the neutral molecule.[18] For V(TCNE)$_x$, three features can be discerned in the binding energy region between 0 and 5 eV. These frontier valence states are composed of the destabilized HOMO and the SOMO of $TCNE^-$ plus the triply occupied 3d level of the V^{2+} ion. We have shown previously that the peak at about 1 eV binding energy related to the highest occupied band of V(TCNE)$_x$ becomes strongly en-

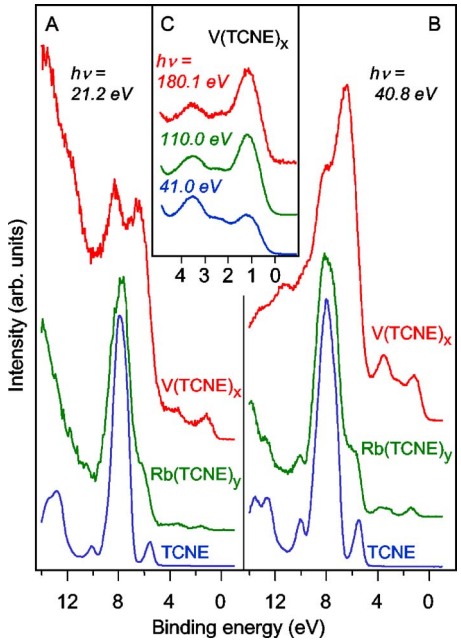

FIG. 4. (Color online) Valence band PES spectra of condensed TCNE, Rb-intercalated TCNE, denoted $Rb(TCNE)_y$, and $V(TCNE)_x$, measured with $h\nu$=21.2 eV (A) and $h\nu$=40.8 eV (B). Panel C shows low binding energy PES spectra of the frontier electronic states of $V(TCNE)_x$ recorded with different photon energies.

hanced in RPE spectra measured at the V L_3-edge, demonstrating that this peak has V($3d$) character. This is also evident from a comparison of valence band PES spectra recorded at increasing photon energies (Fig. 4, panel C). Since the dependence of the photoionization cross sections on $h\nu$ is orbital specific, changes in the relative intensities of the valence band features can be indicative of the corresponding orbital character. The decline of the V($3d$) photoionization cross section with increasing $h\nu$ is considerably slower as that for C($2p$)- and N($2p$)-derived valence states,[22] indicating that the peak that dominates at higher excitation energies is V($3d$)-related.

RPE measurements performed at the C and N K edge showed only weak resonating behavior of the valence states, while most of the spectral weight originated from a competing Auger-like spectator decay process. Nevertheless, a small resonant enhancement could be observed for the frontier valence peaks at 2.5 and 3.5 eV in the RPE spectra recorded at the C K edge.[14] Based on these observations, we assigned the three frontier valence peaks at 1.0, 2.5, and 3.5 eV to V($3d$), $TCNE^-$ SOMO, and $TCNE^-$ destabilized HOMO, respectively. It should be noted however, that the actual situation may be more complex, due to, e.g., hybridization effects and the presence of various bonding configurations, possibly leading to additional, unresolved states. Unfortunately, since the structure of the compound remains so far unknown, a more detailed interpretation of the valence band spectra using theoretical modeling is not possible at present.

The large peak at 8 eV in the neutral TCNE spectra, corresponding to a group of ten molecular orbitals,[23,24] remains essentially unchanged in Rb-intercalated TCNE besides a rigid shift in binding energy, whereas it is split into two spectral features for $V(TCNE)_x$ (Fig. 4, panels A and B). This suggests that stronger reorganization of the occupied valence electronic structure occurs in $V(TCNE)_x$, indicative of a bonding network featuring covalent character, as opposed to the more ionic compound Rb-TCNE.

C. V $L_{2,3}$-edge XAS and XMCD

Figure 5(a) shows V $L_{2,3}$-edge XAS spectra of $V(TCNE)_x$ recorded at room temperature with circularly polarized light impinging on the sample at an angle of 70° with respect to

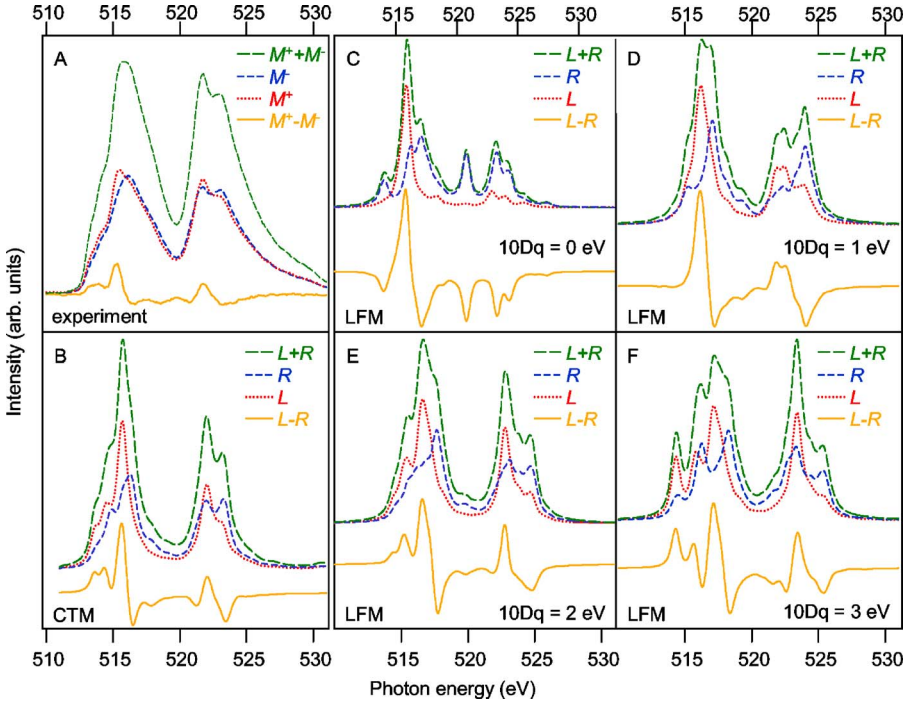

FIG. 5. (Color online) (a) V $L_{2,3}$-edge XAS spectra of $V(TCNE)_x$, denoted M^+ and M^-, measured with a fixed circular polarization of the light and reversed magnetization directions. Also shown are the sum XAS spectrum ($M^+ + M^-$) and the XMCD spectrum ($M^+ - M^-$). (b) CTM calculation of V^{2+} in O_h symmetry; shown are XAS spectra for left (L) and right (R) circularly polarized light, the sum spectrum ($L+R$), and the difference, i.e., XMCD, spectrum (L)-(R). (c)–(f) show the same as (b) but for LFM calculations of V^{2+} in O_h symmetry for different values of $10Dq$.

the sample normal, for opposite in-plane magnetization directions denoted M^+ and M^-. The spectra were recorded in remanence, following a 200 G magnetic field pulse. The XMCD signal, which was acquired by subtracting M^- from M^+, shows that the spins on the V ions are ferromagnetically ordered. The XMCD signal was scaled by a factor of 1.36 $[=1/\cos(30°)/0.85]$ to account for the angle between the photon wave vector and the magnetization direction as well as the degree of circular polarization of the light, which was taken to be 85%.[25]

The XAS spectra are composed of a multitude of lines arising from electric dipole transitions between the $2p$ core levels and empty $3d$ valence states, while additional contributions of $2p\rightarrow 4s$ transitions are negligible. The two main features in the spectra correspond to two groups of multiplets involving $2p_{3/2}$ (L_3-edge) and $2p_{1/2}$ (L_2-edge) states, respectively, separated by the $2p$ spin orbit coupling energy. Due to the strong interaction between the $2p$ core holes and the $3d$ valence electrons in transition metals, the excited states remain strongly localized on the V ions. Consequently, the $L_{2,3}$-edge XAS spectra are closely related to the atomic multiplet structure, allowing accurate description of experiments by ligand field multiplet (LFM) or charge transfer multiplet (CTM) calculations as developed by Thole and co-workers,[26–28] based on Cowan's atomic multiplet code and Butler's group theoretical code.[29,30] In LFM calculations, the interaction with neighboring atoms is taken into account in a simple way by lowering of the ground state symmetry and the introduction of the crystal field, which, for cubic fields, is traditionally parametrized by D_q, D_s, and D_t. In addition, hybridization effects can be modeled by tuning the reduction factor, κ, of the Slater integrals to account for the expansion of the $3d$-derived wave functions in case of increasing covalence of the bonds (the so-called nephelauxetic effect). CTM calculations are used to model hybridization in terms of ligand to metal charge transfer (CT). This scheme employs configuration interaction, in which the electronic states are described as a mixture of $3d^n$ and $3d^{n+1}\underline{L}$, where $\underline{L}$ is a ligand hole.

We will start the discussion of the V L-edge XAS and XMCD spectra of $V(TCNE)_x$ using LFM calculations of V^{2+} ions in a cubic crystal field (O_h symmetry) arising from the nitrogen ligands of $TCNE^-$ [see Figs. 5(c)–5(f)]. This is a reasonable starting point based on extended x-ray absorption fine structure (EXAFS) studies by Haskel *et al.* that have shown that the V^{2+} ions are coordinated to 6.04 ± 0.25 nitrogen atoms,[20] which strongly points to an octahedral bonding environment. The observation of a pre-edge feature at the V K-edge by the same authors supports the model of V^{2+} situated in a weakly distorted octahedron. Figures 5(c)–5(f) display calculated curves for excitation with left- and right-circularly polarized light, denoted L and R, the sum spectra $L+R$, and the corresponding XMCD curves $L-R$, while $10Dq$ is changed from 0 eV [representing the isolated ion in $O(3)$ symmetry] to 1, 2, and 3 eV. The Hartree-Fock Slater integrals were scaled to 80% of their atomic values to account for some covalency of the bonds between the V^{2+} ions and the cyano ligands. A convolution of Lorentzian ($\sigma=0.3$ eV) and Gaussian ($\sigma=0.15$ eV) broadening was applied to each line in the calculated XAS spectra. It should be noted that the calculations cannot be used to produce appropriate absolute energy values.[31]

A comparison of the spectral features obtained by the LFM calculations for different $10Dq$, while disregarding the differences in the experimental versus calculated XMCD intensities for the time being, shows that the experiment is best described by the simulation with a relatively high crystal field strength of $10Dq=2$ eV. At lower values, e.g., $10Dq=1$ eV, the first XMCD feature below 515 eV excitation energy in the experimental data is no longer reproduced, whereas at even higher values a clear peak should split off from the main L_3 feature in the XAS spectra toward lower energies. Upon setting $10Dq$ to 2 eV, all the peaks in the XMCD curve can be reproduced and a reasonable agreement between experimental and calculatd XAS spectra can be observed. Our results are thus fully consistent with the picture of V^{2+} ions in an octahedral bonding environment. It should be pointed out that small distortions of the octahedron, modeled by lowering the symmetry to C_{4h} and introducing finite values for D_s and D_t, does not lead to significant changes in the spectral shapes.

So far, we have largely neglected the issue of covalence of the V-NC bonds. It turns out, however, that it is necessary to include configuration interaction to reproduce both the XAS and XMCD features more precisely. A simple reduction of κ (i.e., below 0.8), which in some cases works well to model the effects of covalency in hybrid bonds,[32] did not produce good results. The curves obtained by such a CMT calculation, in which the parameters were optimized to obtain a good agreement between theory and experiment, are shown in Fig. 5(b). The initial and final states were constructed as a linear combination of two configurations, e.g., for the initial state $|\Psi_i\rangle=\alpha|3d^n\rangle+\beta|3d^{n+1}\underline{L}\rangle$. Although the calculation describes the main features of the XAS and XMCD spectra very well [see Figs. 5(a) and 5(b)], the experimental L_2- and L_3-edge show increased spectral weight tailing towards higher energy, which might be indicative of additional admixed CT configurations, or could be related to inhomogeneous bonding environments. Since it is not possible to resolve any individual features in the high energy tails, we did not attempt to include more than two configurations in the calculations. The ground state charge transfer energy, defined as the difference between the energies of the $3d^{n+1}$ and $3d^n$ states was optimized to $\Delta=1$ eV. The final state charge transfer energy is given by $\Delta'=\Delta+U_{pd}+U_{dd}$, where U_{pd} is the core-hole potential and U_{dd} is the repulsion between the d electrons. Since U_{pd} is about 1 to 2 eV larger than U_{dd},[33] we set Δ' to 0 eV. The ligand to metal charge transfer is further characterized by a transfer integral of the form $T=\langle 3d^n|H|3d^{n+1}\underline{L}\rangle$,[34] which is different for t_{2g} versus e_g states. In transition metal oxides, for which σ-bonding is most important, the transfer integral is larger for the e_g orbitals that point towards the ligands and a ratio of $T_{eg}/T_{t2g}=2$ is commonly applied.[35,36] In $V(TCNE)_x$, the V-cyano bonds may be expected to have considerable π character, which would lead to a larger value of T_{t2g}. Indeed it turned out that setting T_{eg}/T_{t2g} between 1 and 0.5 provided reasonable results; the calculation shown here uses $T_{eg}=1.5$ eV and $T_{t2g}=1.9$ eV. The crystal field parameter $10Dq$ was set to 2.3 eV in both initial and final states. It follows from the

calculations that the ground state is a distinct hybrid state, described by a mixture of 60% $3d^3$ and 40% $3d^4\underline{L}$. This result is striking in comparison to previous studies of bimetallic cyanides,[32] in which the nitrogen-M^{2+} bond (M=Ni, Co, Fe, and Mn) was found to result in very little charge transfer (ground state 90% $3d^n$ type). This might indicate that V^{2+} ions form a special case in the transition metal series, consistent with the robust magnetic ordering temperatures found for $V(TCNE)_x$.

As a final point, we address the XMCD intensity difference between theory and experiment. It is clear that the experimentally observed XMCD effect is small compared to the calculations, which show that the remanent magnetization M_r deviates significantly from the saturation value M_s. This observation is in line with previously published studies of the magnetic properties of $V(TCNE)_x$ thin films prepared by CVD methods,[13] which showed that M_r of such films at room temperature was less then 5% of the saturation magnetization at 5 K. In the present case, M_r seems to be significantly larger. The MCD ratio, i.e., $(L-R)/(L+R)$ or $(M^+-M^-)/(M^++M^-)$, at the L_3-edge is roughly 30% for the calculated spectra (CMT calculation), while it is about 10% in the experiment. Since the MCD ratio has been shown to be directly proportional to the magnetization,[37–41] it can be tentatively concluded that M_r is close to 30% of M_s. The high M_r as compared to the values reported by Pokhodnya *et al.* is most probably related to a reduction of structural disorder in our *in situ* prepared thin film samples. It should be pointed out though that the estimation of M_r is not very precise, due to differences in the experimental and calculated spectral shapes, and the possible presence of an unknown amount of nonmagnetic V.

IV. CONCLUSIONS

Using an *in situ* CVD method and an array of *in situ* electron spectroscopic methods, thin films of $V(TCNE)_x$ were prepared and characterized in UHV. The films were oxygen free within the XPS detection limit of about 0.1 at. %. N($1s$) and C($1s$) XPS spectra clearly indicate the presence of $TCNE^-$, while the asymmetrical shape of the main lines in these spectra is most probably related to the presence of both V-coordinated and uncoordinated cyano groups. Using the XPS V($2p$) peak positions, the charge state of the vanadium ion was assigned as V^{2+}, which is confirmed by LFM and CMT calculations of the XAS and XMCD spectra. XPS shows that, as expected, the carbon to nitrogen ratio in $V(TCNE)_x$ is identical to that in TCNE, although an additional carbon contribution is observed for films that are deliberately oxidized during growth, arising from oxidation products of $V(C_6H_6)_2$. The V:N ratio derived from the XPS data confirms the stoichiometry $V(TCNE^-)_x$ with $x \approx 2$. Room temperature magnetic ordering was confirmed from the observation of a large XMCD signal at the V $L_{2,3}$ edge, measured in remanence. Simulations of the experimental XAS and XMCD curves revealed a large crystal field parameter $10Dq=2.3$ eV and a hybrid V($3d$)-CN ground state given by 60% $3d^3$ and 40% $3d^4\underline{L}$, where $\underline{L}$ is a hole on the cyano ligands. This hybrid orbital character, which is expected to play an important role in the robust magnetic ordering interactions, is consistent with the strong reorganization of the TCNE-derived valence electronic structure in $V(TCNE)_x$ as compared to the model ionic intercalation compound Rb-TCNE.

ACKNOWLEDGMENTS

We thank F. M. F. de Groot for the code to perform LFM and CTM calculations. The authors acknowledge financial support from the Swedish Research Council (VR) and the Carl Tryggers Foundation. In general, research by the two groups at Linköping University is supported by the EU Integrated Project NAIMO (Grant No. NMP4-CT-2004-500355), the Center for Organic Electronics, COE@COIN, and the Center for Advanced Molecular Materials, CAMM, both funded by the Swedish Foundation for Strategic Research.

[1] J. S. Miller, Adv. Mater. (Weinheim, Ger.) **14**, 1105 (2002).
[2] O. Kahn, *Molecular Magnetism* (VCH Publishers, New York, 1993).
[3] S. Blundell and F. Pratt, J. Phys.: Condens. Matter **16**, R771 (2004).
[4] J. S. Miller and A. J. Epstein, MRS Bull. **25**, 21 (2000).
[5] I. Žutić, J. Fabian, and S. Das Sarma, Rev. Mod. Phys. **76**, 323 (2004).
[6] J. Zhang, J. Ensling, V. Ksenofontov, P. Gutlich, A. J. Epstein, and J. S. Miller, Angew. Chem., Int. Ed. **37**, 657 (1998).
[7] C. M. Wynn, M. A. Girtu, J. Zhang, J. S. Miller, and A. J. Epstein, Phys. Rev. B **58**, 8508 (1998).
[8] M. A. Girtu, C. M. Wynn, J. Zhang, J. S. Miller, and A. J. Epstein, Phys. Rev. B **61**, 492 (2000).
[9] J. M. Manriquez, G. T. Yee, R. S. McLean, A. J. Epstein, and J. S. Miller, Science **252**, 1415 (1991).
[10] J. S. Miller and A. J. Epstein, Chem. Commun. (Cambridge) **1998**, 1319.
[11] K. I. Pokhodnya, D. Pejakovic, A. J. Epstein, and J. S. Miller, Phys. Rev. B **63**, 174408 (2001).
[12] P. Zhou, B. G. Morin, J. S. Miller, and A. J. Epstein, Phys. Rev. B **48**, 1325 (1993).
[13] K. I. Pokhodnya, A. J. Epstein, and J. S. Miller, Adv. Mater. (Weinheim, Ger.) **12**, 410 (2000).
[14] C. Tengstedt, M. P. de Jong, A. Kanciurzewska, E. Carlegrim, and M. Fahlman, Phys. Rev. Lett. **96**, 057209 (2006).
[15] V. N. Prigodin and A. J. Epstein, Adv. Mater. (Weinheim, Ger.) **14**, 1230 (2002).
[16] V. N. Prigodin, N. P. Raju, K. I. Pokhodnya, J. S. Miller, and A. J. Epstein, Synth. Met. **135-136**, 87 (2003).
[17] M. P. de Jong, R. Friedlein, S. L. Sorensen, G. Öhrwall, W. Osikowicz, C. Tengsted, S. K. M. Jonsson, M. Fahlman, and W. R. Salaneck, Phys. Rev. B **72**, 035448 (2005).
[18] C. Tengstedt, M. Unge, M. P. de Jong, S. Stafstrom, W. R.

Salaneck, and M. Fahlman, Phys. Rev. B **69**, 165208 (2004).
[19] J. F. Moulder, W. F. Stickle, P. E. Sobol, and K. D. Bomben, *Handbook of X-Ray Photoelectron Spectroscopy* (Perkin-Elmer Corporation, Eden Prairie, 1992).
[20] D. Haskel, Z. Islam, J. Lang, C. Kmety, G. Srajer, K. I. Pokhodnya, A. J. Epstein, and J. S. Miller, Phys. Rev. B **70**, 054422 (2004).
[21] G. Silversmit, D. Depla, H. Poelman, G. B. Marin, and R. De Gryse, J. Electron Spectrosc. Relat. Phenom. **135**, 167 (2004).
[22] J. J. Yeh and I. Lindau, At. Data Nucl. Data Tables **32**, 1 (1985).
[23] V. G. Zakrzewski, O. Dolgounitcheva, and J. V. Ortiz, J. Chem. Phys. **105**, 5872 (1996).
[24] K. N. Houk and L. L. Munchausen, J. Am. Chem. Soc. **98**, 937 (1976).
[25] A. Hahlin, Ph. D. thesis, Uppsala University (2003).
[26] B. T. Thole, G. Van Der Laan, and P. H. Butler, Chem. Phys. Lett. **149**, 295 (1988).
[27] K. Okada, A. Kotani, and B. T. Thole, J. Electron Spectrosc. Relat. Phenom. **58**, 325 (1992).
[28] K. Okada, A. Kotani, H. Ogasawara, Y. Seino, and B. T. Thole, Phys. Rev. B **47**, 6203 (1993).
[29] R. D. Cowan, *The Theory of Atomic Structure and Spectra* (University of California Press, Berkely, 1981).
[30] P. H. Butler, *Point Group Symmetry Applications: Methods and Tables* (Plenum, New York, 1981).
[31] F. M. F. de Groot, J. C. Fuggle, B. T. Thole, and G. A. Sawatzky, Phys. Rev. B **42**, 5459 (1990).
[32] M.-A. Arrio, P. Sainctavit, C. Cartier dit Moulin, T. Mallah, M. Verdaguer, F. Pellegrin, and C. T. Chen, J. Am. Chem. Soc. **118**, 6422 (1996).
[33] F. M. F. de Groot, Chem. Rev. (Washington, D.C.) **101**, 1779 (2001).
[34] Z. Hu, C. Mazumdar, G. Kaindl, F. M. F. de Groot, S. A. Warda, and D. Reinen, Chem. Phys. Lett. **297**, 321 (1998).
[35] L. F. Mattheiss, Phys. Rev. B **5**, 290 (1972).
[36] F. M. F. de Groot, J. Electron Spectrosc. Relat. Phenom. **67**, 529 (1994).
[37] G. Schutz, W. Wagner, W. Wilhelm, P. Kienle, R. Zeller, R. Frahm, and G. Materlik, Phys. Rev. Lett. **58**, 737 (1987).
[38] C. T. Chen, F. Sette, Y. Ma, and S. Modesti, Phys. Rev. B **42**, 7262 (1990).
[39] T. Koide, T. Shidara, H. Fukutani, K. Yamaguchi, A. Fujimori, and S. Kimura, Phys. Rev. B **44**, 4697 (1991).
[40] J. G. Tobin, G. D. Waddill, and D. P. Pappas, Phys. Rev. Lett. **68**, 3642 (1992).
[41] B. T. Thole, P. Carra, F. Sette, and G. van der Laan, Phys. Rev. Lett. **68**, 1943 (1992).